Journal of Electroceramics (2021) 46:141–150
https://doi.org/10.1007/s10832-021-00255-6

Effect of Mn/Nb heterovalent substitution on the electrocaloric response and energy storage performance of Ba(Sn, Ti)O_3 relaxor-ferroelectrics

Ying Hou[1] · Jiacheng Li[1] · Sheng Guo[1] · Tingting Ye[2] · Junfeng Ding[2]

Received: 2 February 2021 / Accepted: 2 July 2021 / Published online: 16 July 2021

Abstract
Electrocaloric (EC) refrigeration, is accepted as an auspicious method to develop eco-friendly cooling devices. Here, the investigations on the EC response and energy storage performance of heterovalent-doped Ba(Sn, Ti)O_3 relaxor ferroelectrics are carried out. Doping of aliovalent Mn or Nb elements into Ti site would regulate both the EC and energy storage behaviors. An enhanced EC temperature change up to 1.31 K, and a maximal recoverable energy storage density of 0.24 J cm^{-3} with the efficiency as high as 87.11 %, can be observed under 70 kV cm^{-1} in 0.5 % acceptor-doped Ba(Sn, Ti)O_3 ceramics. It is found that the local internal stress, the local charge fluctuation, and the oxygen deficiencies would benefit the electrical behaviors of this system. These results would shed light on the effect of the heterovalent substitution on the electrical properties of lead-free $BaTiO_3$ system and provide a novel and simple route to further improve the EC response and energy storage performance.

Keywords Electrocaloric · Energy storage · Relaxor ferroelectrics · Heterovalent doping

1 Introduction

Since the discovery of ferroelectrics, ferroelectric materials have been exploited in abundant applications, such as memories, energy harvestors, and so on [1, 2]. Recently, ferroelectrics, especially relaxor ferroelectrics, have been considered as the potential candidates for the electrocaloric (EC) solid-state cooling prototypes, which is a highly efficient and environmentally benign refrigeration technology [3–6]. Here, the electrocaloric effect (ECE) is defined as the adiabatic change in entropy (ΔS)/ temperature (ΔT) caused by the operation of an external electric field in ferroelectrics.

Aiming at achieving the high EC response with low voltage required and near room temperature, a great number of researches focus on the search of environmental friendly electrocalorics, such as lead-free $BaTiO_3$-based ceramics [7, 8], and the investigation of the strategies for improving the EC response, for instance, maximizing the number of coexisting phases [9, 10]. It has been reported that the coexistence of multiple phases near an invariant critical point (ICP) would lead to a significant increase of the entropy and meanwhile broaden the effective temperature range of ECE in Zr and Sn hybrid doped $BaTiO_3$ relaxor ferroelectrics [11]. In addition, modified $BaTiO_3$ system with different isovalent substituting elements such as Ca^{2+}, Sr^{2+} substituted Ba site [12, 13], or Hf^{4+}, Ce^{4+} doped Ti site [14, 15], have also been widely reported to further improve the EC response. Furthermore, a little bit of attention has recently been paid to the heterovalent substitution which would introduce the oxygen or cation vacancies in the system. For example, a large EC response can be observed by the aliovalent substitution of Y and Mn into $BaTiO_3$ [16]. Additionally, the co-doping of the donor Ce^{3+} into Ba site and the acceptor Mn^{3+} into Ti site would improve the EC response and broaden the operating temperature range, by regulating the oxygen vacancies and the grain size of ceramics [17]. These results illustrate that the ECE would be effectively enhanced and regulated through the aliovalent substitution in $BaTiO_3$ system.

Since the introduction of the heterovalent element into Ba or Ti site would induce oxygen or cation vacancies, the dielectric permittivity and the polarization of this system would change subsequently [18]. The energy storage performance has been confirmed to be closely dependent on the

✉ Ying Hou
houying@ecust.edu.cn

[1] Department of Physics, East China University of Science and Technology, Shanghai 200237, China

[2] Key Laboratory of Materials Physics, Institute of Solid State Physics, Chinese Academy of Sciences, Hefei 230031, China

ferroelectric behaviors [19], and thus the energy storage density and efficiency could also be tunable by the aliovalent dopants into Ba or Ti site of $BaTiO_3$ ceramics.

In this work, the heterovalent-substitution dependent on the dielectric, ferroelectric, electrocaloric, and energy storage behaviors have been systematically investigated through acceptor Mn^{2+}/Mn^{3+} or donor Nb^{5+} doping into Ti^{4+} site of Ba(Sn, Ti)O_3 ceramics. It is found that both the electrocaloric and energy storage performances can be effectively regulated by the replacement of only 0.5 % Ti with aliovalent elements, and more significantly, these properties are obviously enhanced in 0.5 % Mn-doped $BaTiO_3$ system.

2 Materials and methods

The $BaSn_{0.11}Ti_{0.89-x}M_xO_3$ ($x = 0$, 0.005, and 0.01, M = Mn or Nb) ceramics were prepared by the solid-state reaction method. High purity reagents $BaCO_3$ (99 % pure), TiO_2 (99 % pure), SnO_2 (99 % pure), MnO (99 % pure), and Nb_2O_5 (99 % pure) powders were used. The stoichiometric precursors were grinded to achieve the uniform mixture and then calcined at 1100 °C for 2 h to stimulate the solid-state reaction. Followed by further milling, the powders were pressed into a disk shaped pellet of 12 mm diameter and 1 mm thickness, after mixing with 5 wt% polyvinyl alcohol (PVA) solution. The pellets were further sintered at 1400 °C~1450 °C for 2 h.

X-ray diffraction data of sintered powders were obtained using an X-ray diffractometer (Model X'Pert PRO, PANalytical, Almelo, Holland) with Cu Kα radiation. The surface morphology was observed by a scanning electron microscope (SEM, Model JSM6380-LV, JEOL, Tokyo, Japan). Prior to microstructural analysis, the ceramic samples were fine-polished and then thermal etched at 1300 °C for 1 h [20–23]. For electrical measurements, silver electrodes were used on the polished surfaces of the ceramics. The dielectric properties were measured by an E4980A impedance analyzer (Agilent, USA). Furthermore, the ferroelectric behavior was carried out using ferroelectric analyzer (TF2000, aix-ACCT, Aachen, Germany).

3 Results

3.1 Structural and morphological properties

The XRD patterns of $BaSn_{0.11}Ti_{0.89}O_3$ (BST), $BaSn_{0.11}Ti_{0.885}Mn_{0.005}O_3$ (BSTMn0.005), $BaSn_{0.11}Ti_{0.88}Mn_{0.01}O_3$ (BSTMn0.01), $BaSn_{0.11}Ti_{0.885}Nb_{0.005}O_3$ (BSTNb0.005), and $BaSn_{0.11}Ti_{0.88}Nb_{0.01}O_3$ (BSTNb0.01) ceramics recorded at room temperature are displayed in Fig. 1. As these results indicated, all the samples have a pure perovskite structure without any

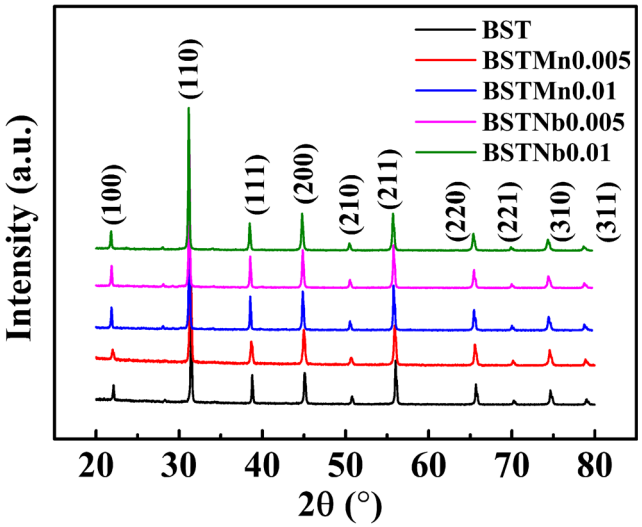

Fig. 1 (color online) XRD patterns of BST, BSTMn0.005, BSTMn0.01, BSTNb0.005, and BSTNb0.01 ceramics recorded at room temperature

secondary phase or impurities, and exhibit tetragonal phase with P4mn space group. With the introduction of Mn/Nb dopants, all the diffraction peaks shift to the lower angle and thus the lattice parameters increase in the Mn/Nb-modified BST system, which is caused by the larger-sized doping ions (Mn^{2+}: 0.067 nm and Nb^{5+}: 0.064 nm) than the equivalent radius of 0.0614 nm for B-site ions consisted of 89 %Ti^{4+} (0.0605 nm) and 11 %Sn^{4+} (0.069 nm). It means that the solid state reaction has occurred in the specified sintering condition and the doping Mn^{2+} and Nb^{5+} ions all enter into Ba(Sn, Ti)O_3 lattice.

Figure 2 shows the surface SEM images of BST, Mn or Nb-doped BST ceramics. It can be seen that all these samples are dense and the average grain sizes are around 1 μm for BST ceramics, 3 ~ 4 μm for BSTMn0.005 and BSTNb0.005, and 1 ~ 3 μm for BSTMn0.01 and BSTNb0.01. It is clear that the relatively larger grain size exists in 0.5 % Mn/Nb-doped BST ceramic samples. As we know, the Mn/Nb entering into the Ti site would cause the formation of the oxygen vacancies/cation vacancies. The vacant sites would be helpful for the mass transportation, which might be responsible for the larger grain size in 0.5 % Mn/Nb-doped BST system [17]. However, when the Mn/Nb content is increased up to 1 %, a part of Mn/Nb would accumulate at the grain boundaries, which would hinder the further motion of grain boundaries and the further growth of the grains [24].

3.2 Dielectric and ferroelectric properties

The temperature dependences of the dielectric permittivity at different frequencies for BST, and Mn/Nb doped BST are shown in Fig. 3. The temperature at which the dielectric constant reaches a maximum value and the maximum permittivity are assigned to be T_m and ε_m, respectively. The values of T_m and ε_m for all these ceramics are compared in Table 1. It is

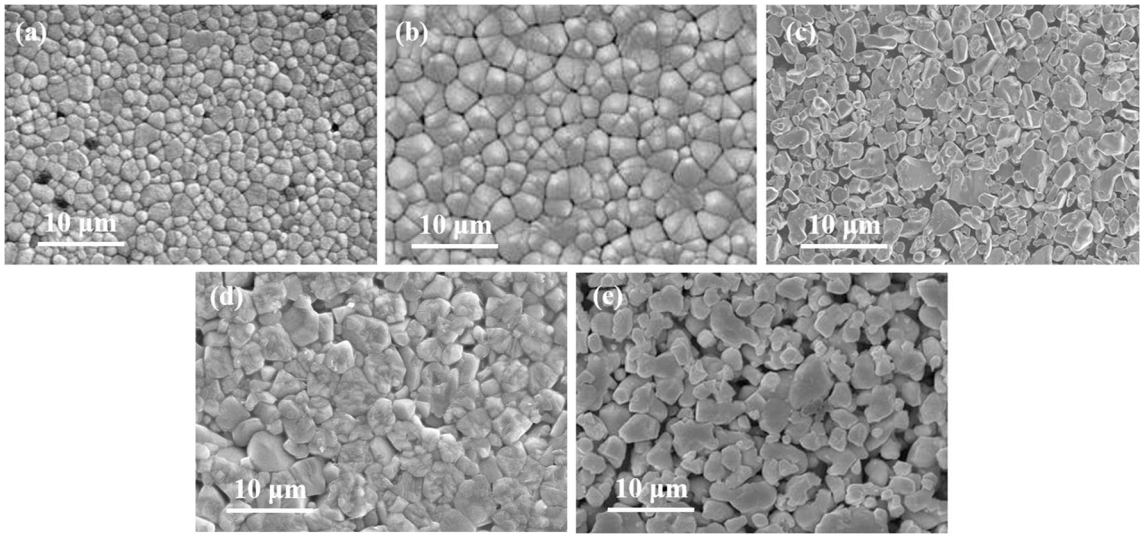

Fig. 2 The surface SEM images of BST (**a**), BSTMn0.005 (**b**), BSTMn0.01 (**c**), BSTNb0.005 (**d**), and BSTNb0.01 (**e**)

found that the maximum dielectric permittivity of 3889 for BST is lower than that reported in the previous studies [25, 26], since the dielectric behaviors are closely dependent on the grain sizes and microstructures [27–29], and SEM images display relatively small grain sizes in this system (1 μm for BST ceramics, 3 ~ 4 μm for BSTMn0.005 and BSTNb0.005, and 1 ~ 3 μm for BSTMn0.01 and BSTNb0.01). In addition, the highest ε_m exists in BSTMn0.005 ceramics, illustrating that the improved ECE and energy storage can be expected in the 0.5 %-doped BST system. The dielectric properties display a relaxor-like ferroelectric behavior, since all the samples display the broad peaks at T_m and the values of T_m shifts to higher temperature with the increasing frequency. The fact that the decreasing T_m with the increase of the Mn/Nb content further confirms that the Mn/Nb is successfully doped into Ti/Sn site [30]. It is found that Nb doping would increase the relaxor behaviors and broaden the transition temperature range [18, 31].

Following the Curie-Weiss law described as

$$\frac{1}{\varepsilon_r} = \frac{T - T_0}{C} \tag{1}$$

the dielectric behaviors above T_m can be fitted. In Eq. (1), ε_r represents the dielectric constant, T_0 is the Curie-Wiess temperature for the second phase transition, and C is the Curie constant. The fitting parameter C is $9.16 \cdot 10^4$ K for BST, $9.55 \cdot 10^4$ K for BSTMn0.005, $1.04 \cdot 10^5$ K for BSTMn0.01, $1.08 \cdot 10^5$ K for BSTNb0.005, and $1.28 \cdot 10^5$ K for BSTNb0.01, respectively. These fitting parameters will be useful for calculating the ECE of this system.

In order to further evaluate the EC response and energy storage performance, the polarization-electric field (*P-E*) hysteresis loops at various temperatures (300 K ~ 358 K) for these ceramics are tested under different electric fields and at an increment of 5 K, as shown in Fig. 4. The test frequency is 10 Hz for all of these measurements. The typical relaxor-ferroelectric hysteresis loops are achieved for all these samples, according with the dielectric results. However, the leakage exists around room temperature in BSTMn0.01 and BSTNb0.01 (see Fig. 4(c) and (e)), due to the ionic accumulation at the grain boundaries, and the more electrovalent mismatch and the charge fluctuation in samples with more heterovalent dopants. It is found that the shapes of *P-E* loops shrink and the intensities of the polarization decrease as the temperature increases. The polarization decreases slightly with the increasing temperature, confirming the relaxor behavior of this system.

The room-temperature polarizations of these ceramics under 80 kV cm^{-1} are listed in Table 1. 0.5 % Mn substituted BST exhibits the enhanced polarization compared with other samples. Combined with the largest ε_m in BSTMn0.005, the dielectric and polarization results demonstrate that the EC response would be improved by introducing the heterovalent 0.5 % Mn into BST relaxors.

3.3 Electrocaloric effect

Based on *P-E* loops and dielectric behaviors, the ECE, i.e., the entropy change (ΔS) and the temperature change (ΔT) under applied electric fields, can be evaluated by the indirect methods from Maxwell equations and Landau-Ginzburg-Devonshire (LGD) phenomenological theory as follows [25, 32, 33]

$$\Delta S = \frac{1}{\rho}\int_{E_1}^{E_2}\left(\frac{\partial P}{\partial T}\right)_E dE \tag{2}$$

$$\Delta T = -\frac{1}{\rho}\int_{E_1}^{E_2}\frac{T}{c_E}\left(\frac{\partial P}{\partial T}\right)_E dE \tag{3}$$

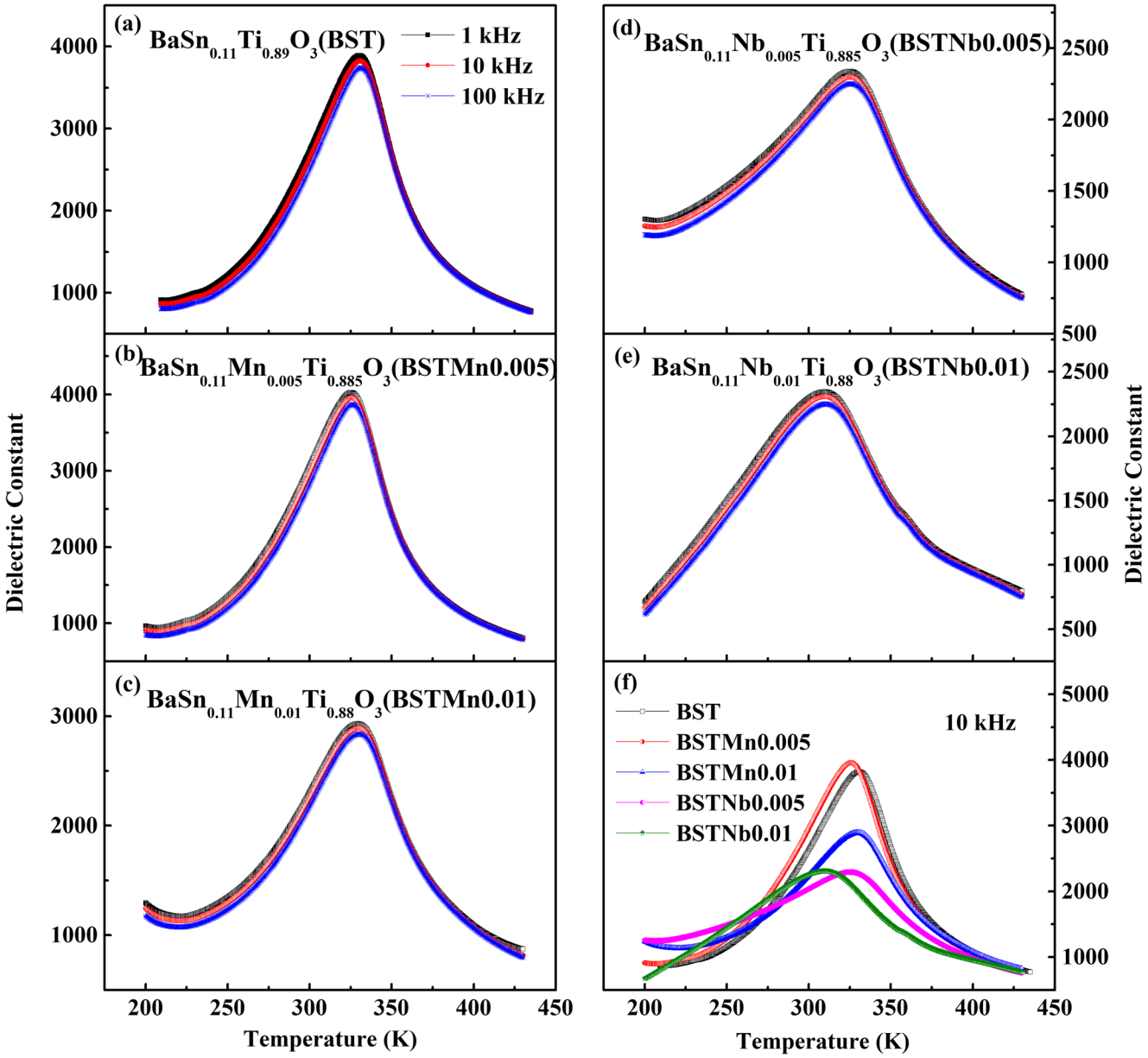

Fig. 3 (color online) The temperature dependence of the dielectric permittivity at different frequencies for BST (**a**), BSTMn0.005 (**b**), BSTMn0.01 (**c**), BSTNb0.005 (**d**), and BSTNb0.01 (**e**) ceramics. The comparison of the permittivity tested at 10 kHz for all these samples is shown in (**f**)

Table 1 The comparison of the dielectric, ferroelectric, electrocaloric, and energy storage performances of Mn/Nb-doped Ba(Sn, Ti)O_3 ceramics

Sample	T_m (K)	ε_m	P (μC cm^{-2})	$\lvert\Delta T\rvert_m$ (K)# (Maxwell)	$\lvert\Delta T\rvert_m$ (K)# (LGD)	W_1 (J cm^{-3})	η (%)
BST	333	3889	10.28	0.63 (333 K)	0.91(333 K)	0.17	54.67
BSTMn0.005	326	3956	11.91	0.72 (328 K)	1.31(328 K)	0.22	71.93
BSTMn0.01	329	2891	15.00 *	-	-	-	-
BSTNb0.005	327	2295	6.39	0.41 (333 K)	0.30(333 K)	0.14	68.18
BSTNb0.01	311	2309	8.03 *	-	-	-	-

*The electric leakage exists in these two samples

Here, $|\Delta T|$ is calculated by Maxwell or LGD under 70 kV cm^{-1}

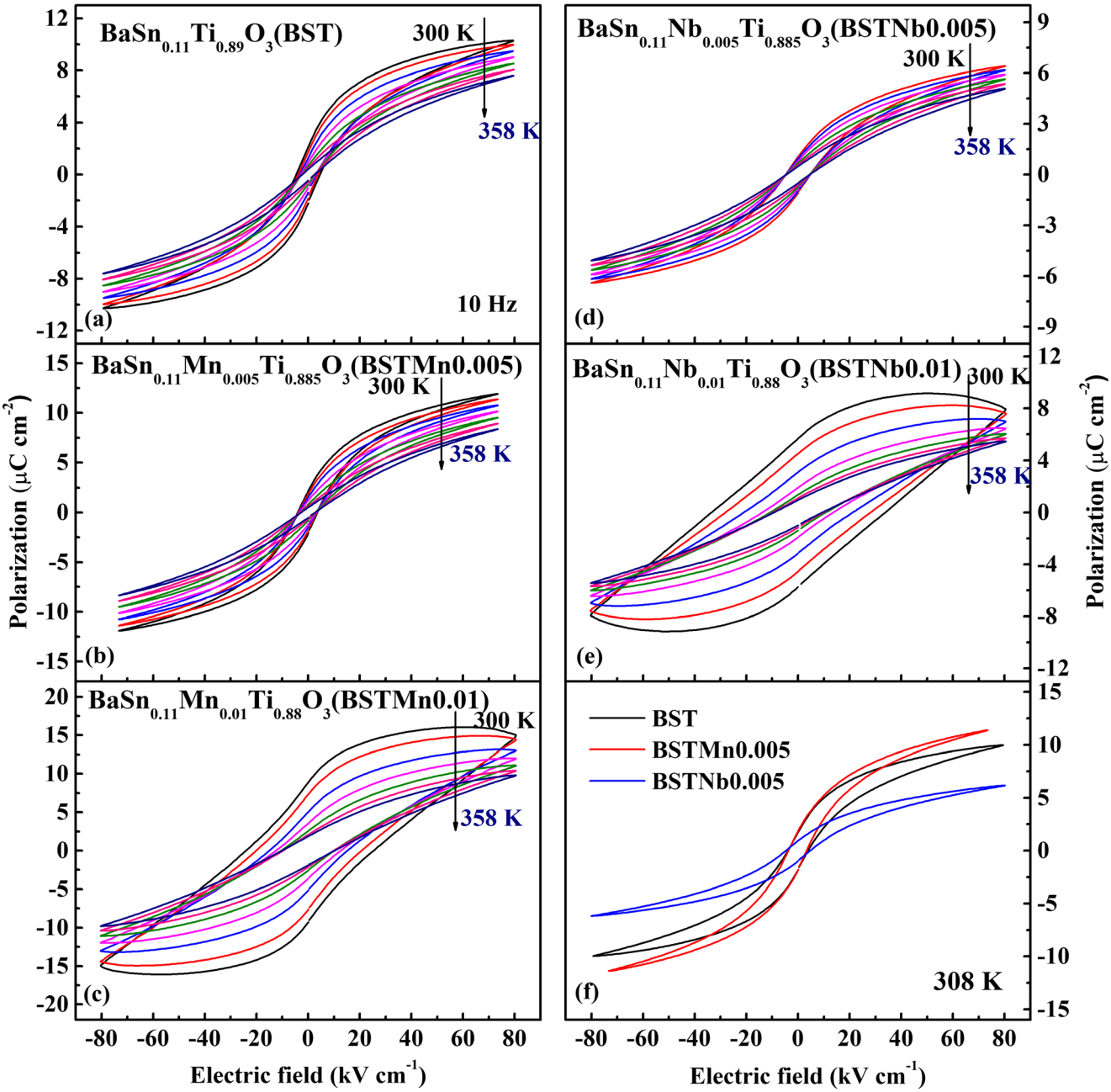

Fig. 4 (color online) The *P-E* hysteresis loops of BST, and Mn/Nb-doped BST samples, recorded at different temperatures

$$\Delta S = -\frac{1}{2}[\beta(T)P^2(E,T) - \beta(T)P^2(0,T)] \quad (4)$$

$$\Delta T = \frac{T}{2c_E}[\beta(T)P^2(E,T) - \beta(T)P^2(0,T)] \quad (5)$$

where ρ is the density and c_E is the specific heat capacity of the ceramics; T is the ambient temperature; E_1 and E_2 are the initial and final applied fields, respectively, where $E_1 = 0$ and E_2 are the maximum applied fields in this work. Here, $\beta = (\varepsilon_0 C)^{-1}$, which is related to the Curie constant C, is considered as a temperature-independent coefficient.

Following Maxwell relations (Eqs. (2) and (3)) and LGD theory (Eqs. (4) and (5)), the changes in polarization and permittivity would reflect the corresponding changes in the entropy and the temperature as well. Figures 5 and 6 depict the variations of $|\Delta T|$, deduced by Maxwell relations and LGD respectively, as a function of the measured temperature for three ceramic samples. As 1 % Mn/Nb doped BST samples exhibit electric leakage in *P-E* loops, the calculated $|\Delta T|$ of these two ceramics may not be accurate. Hence, the EC responses of BSTMn0.01 and BSTNb0.01 are not present for comparison. As expected, the EC response is enhanced by the

increase in the magnitude of the applied electric field. As shown in Fig. 5, all the samples display maximum $|\Delta T|$, which is denoted as $|\Delta T|_m$ in Table 1. One can see that the obtained $|\Delta T|$ of 0.15 K at 20 kV/cm is much lower than that in the previous report [34], because the deduced ECE following indirect methods are strongly dependent on the dielectric and ferroelectric properties however the values of the dielectric permittivity and the ferroelectric polarization are suppressed by the relatively smaller grain size. In Fig. 5(d) we compare the temperature dependent EC response of BST and 0.5 % Mn/Nb doped BST, deduced by Maxwell relations. It is seen that in 0.5 % Mn-doped BST, $|\Delta T|_m$ reaches 0.72 K, at 328 K and at an applied field of 70 kV cm^{-1}, while the values of $|\Delta T|_m$ are 0.63 K for BST and 0.41 K for 0.5 % Nb-doped BST. Here, the EC strength ($|\Delta T|_m/|\Delta E|$) of BSTMn0.005 achieves $0.1 \cdot 10^{-6}$ KmV^{-1}. It is interesting to note that the temperatures at which $|\Delta T|_m$ appears are corresponding to the T_m obtained from dielectric properties. Based on the Maxwell relations, EC responses are closely associated with $\left(\frac{\partial P}{\partial T}\right)_E$, hence the $|\Delta T|$ would be sensitive to the changes of the polarization with the temperature and the variation around the transition temperature would be more obvious than that at other temperatures. Therefore, the optimum EC response over a broad temperature range (300 K ~ 358 K) is obtained in heterovalent-substituting BST with Mn content of 0.5 %, compared with that of BST and BSTNb0.005.

However, since the Maxwell relations are derived based on the reversible and ergodic thermodynamic process, the Maxwell relations would not be accurate if it is applied to relaxor ferroelectrics such as Sn, Mn/Nb-doped $BaTiO_3$ system discussed here [32, 35–37]. Thus, the ECE deduced based on LGD thermodynamic theory, which is widely utilized to describe the macroscopic phenomena that occur in the polar materials, is shown in Fig. 6. One can see that both methods show the same trend with a maximum around the phase transition temperature (328 K ~ 333 K). In Fig. 6(d) we also compare the EC response deduced by LGD model for three ceramics, and it is found that a high cooling value of 1.31 K, and a large EC strength of $0.19 \cdot 10^{-6}$ KmV^{-1}, are achieved in 0.5 % Mn-doped BST, at the temperature of 328 K. Specifically, following LGD model, a wide temperature range (300 K ~ 358 K) EC response can also be observed in this sample, which is highly desirable for cooling devices.

3.4 Energy storage performance

In order to compare the energy storage performance of $BaSn_{0.11}Ti_{0.89}O_3$ ceramics with different dopants, the energy storage density (W_1) and energy storage efficiency (η) have been calculated by using the data generated from *P-E* loops, based on the following two formula

$$W_1 = \int_{P_r}^{P_{max}} EdP \tag{6}$$

$$\eta = \frac{W_1}{W_1 + W_2} \times 100\% \tag{7}$$

where E is the applied electric field, P is the polarization, P_r and P_{max} are the remnant polarization and the maximum polarization respectively, and W_2 represents the energy loss density. The temperature dependence of the energy storage density and efficiency for 0.5 % Mn/Nb-doped BST ceramics is displayed in Fig. 7, and the values of W_1 and η at room temperature are further compared in Table 1. Through the introduction of 0.5 % Mn, both the energy storage density and the efficiency are effectively improved over the whole tested temperature range. Only 0.5 % content of Mn in BST ceramics can increase the room-temperature energy storage density up to 29 % improvement, and the efficiency 32 % improvement, compared with the energy storage performance of BST. The maximum energy storage density of 0.24 J cm^{-3} at 343 K and under 70 kV cm^{-1} can be obtained in BSTMn0.005, and meanwhile the maximal efficiency reaches a level as high as 87.11 %, illustrating that the greater energy storage performance exhibits in Mn-doped system. However, as shown in Fig. 7(d), the partial replacement of Ti by Nb would suppress the energy storage density and efficiency as well.

Table 2 compares the EC response and energy storage performances of the BST, BSTMn0.005, and BSTNb0.005 prepared in this study with those of the lead-free ferroelectric materials (especially $BaTiO_3$-based ceramics). It can be seen that the acceptor-doped $Ba(Sn, Ti)O_3$ in this work, i.e., BSTMn0.005, exhibits both the superior EC and energy storage behaviors: the fact that the maximal EC response of 1.31 K, energy storage density of 0.24 J cm^{-3} and efficiency of 87.11 % can be induced by an applied electric field of 70 kV cm^{-1}, is comparable or even higher than those of other $BaTiO_3$-based lead-free ceramics.

4 Discussion

As mentioned above, compared with BST and Nb-doped BST ceramics, the 0.5 % Mn-doped BST samples show the enhanced electrocaloric and energy storage performances. For Mn/Nb-doped BST samples, the element Mn, substituted for B-site Ti^{4+}, would mainly exist as acceptor Mn^{2+} and Mn^{3+} [45], while Nb would be successfully incorporated as donor Nb^{5+} into Ti^{4+} site [24]. The small amount (0.5 %) of aliovalent doping such as Mn^{2+}, Mn^{3+}, or Nb^{5+}, would induce the local internal stress due to the local size mismatch, and the local charge fluctuation due to the local charge imbalance.

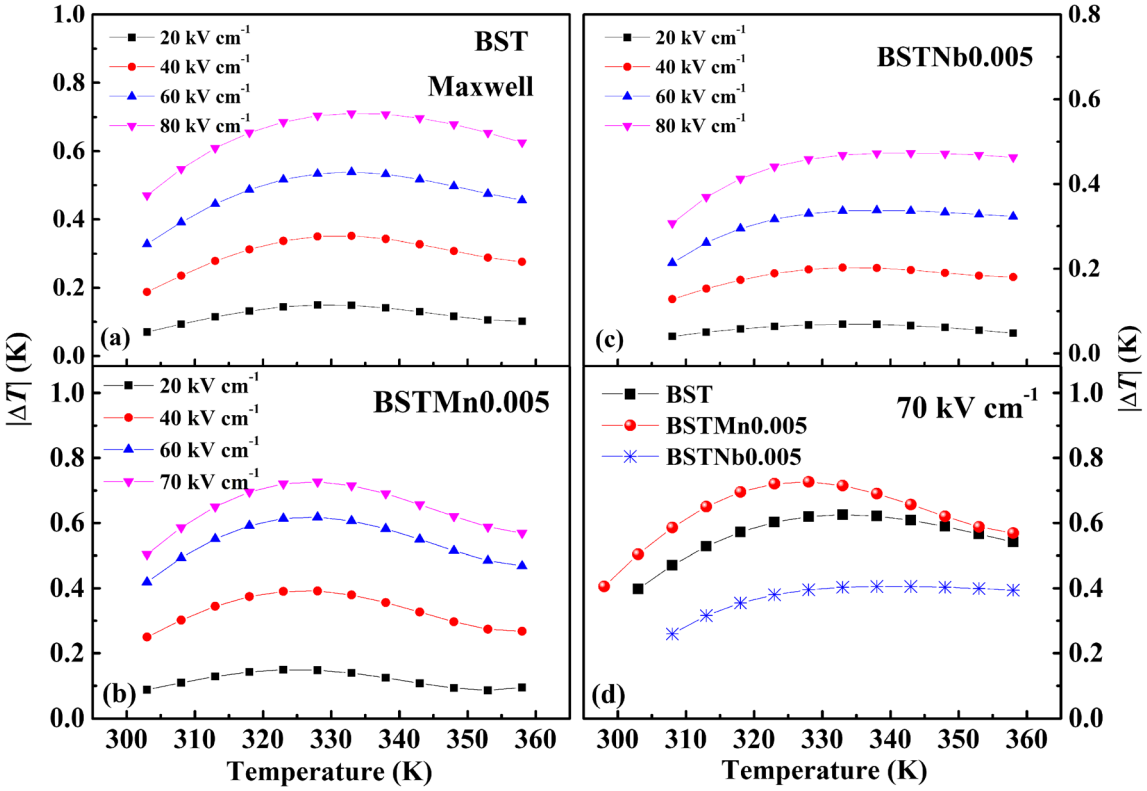

Fig. 5 (color online) The temperature dependence of the electrocaloric response for BST and Mn/Nb-doped BST samples, deduced by Maxwell relations

These local internal stress and local charge fluctuation would be beneficial for the polarization response, EC response and energy storage performance as well. While, the higher content (1 %) of aliovalent dopants could introduce the ionic accumulation, and the random electric fields and the random strain field, which would depress the polarization [46]. Thus, the *P*-*E* loops of BSTMn0.01 and BSTNb0.01 exhibit electric leakage around room temperature.

On the other hand, the introduction of acceptor Mn^{2+} and Mn^{3+} dopants would cause the formation of oxygen

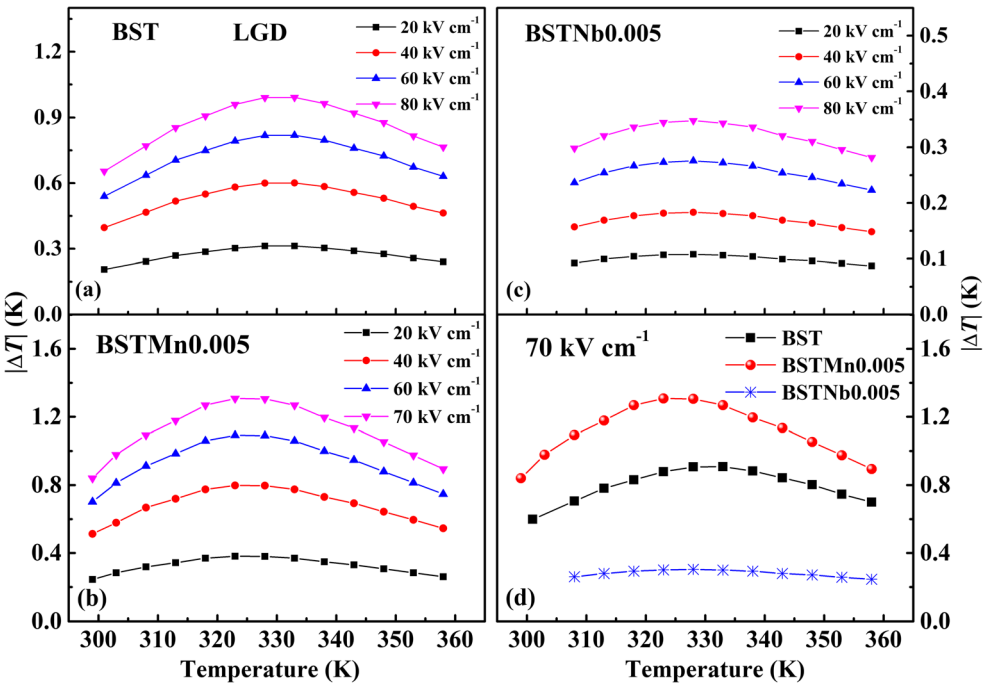

Fig. 6 (color online) The temperature dependence of the electrocaloric response for BST and Mn/Nb-doped BST samples, evaluated using Landau-Ginzburg-Devonshire (LGD) phenomenological theory

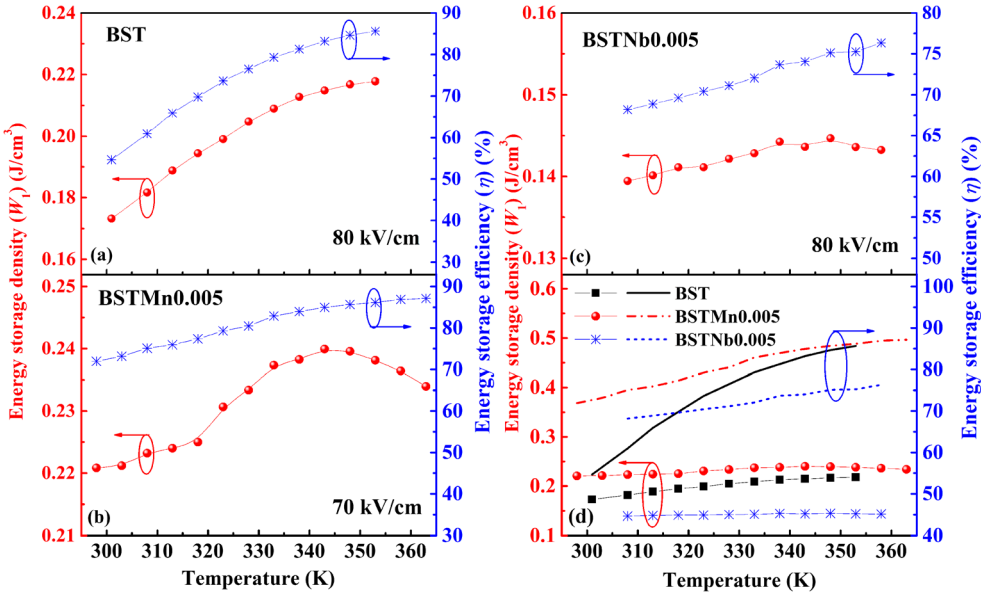

Fig. 7 (color online) The temperature dependence of the energy storage density and efficiency for BST and Mn/Nb-doped BST samples

vacancies. The small ratio of oxygen vacancies could help the mass and cation transportation, which would ease the domain switching and subsequently raise the dielectric and ferroelectric responses [17]. It explains that the improved dielectric permittivity and ferroelectric polarization exhibit in tiny-amount (0.5 %) Mn-doped BST ceramics. Nevertheless, when the composition of Mn ions increases as well as the ratio of oxygen vacancies becomes higher, then the oxygen vacancies would pin the movement of the ferroelectric domain walls and subsequently reduce the dielectric and ferroelectric responses in 1 % Mn-doped BST samples [47–49]. Meanwhile, the donor Nb^{5+} doping induces the diffuse transition behavior and reduces the polarization [31].

Therefore, attributed to the two effects mentioned above, the enhanced dielectric, ferroelectric, electrocaloric, and energy storage behaviors can be observed in lower-content Mn-doped BST samples. While in the Nb-doped BST, these properties are depressed, because the donor doping could affect the

Table 2 Comparison of EC and energy storage performances of Mn/Nb modified-Ba(Sn, Ti)O_3 ceramics with those of other lead-free ceramics (especially $BaTiO_3$-based ceramics) obtained in the literature

ceramics	E (kV cm^{-1})	$\|\Delta T\|$ (K)	EC method	W_1(J cm^{-3})	η (%)	Ref.
$BaSn_{0.11}Ti_{0.89}O_3$	70	0.63(@333K) 0.91(@333K)	Maxwell LGD	0.17(@RT) 0.21(@353K)	54.67(@RT) 85.64(@353K)	this work
$BaSn_{0.11}Ti_{0.885}Mn_{0.005}O_3$	70	0.72(@328K) 1.31(@328K)	Maxwell LGD	0.22(@RT) 0.24(@343K)	71.93(@RT) 87.11(@363K)	this work
$BaSn_{0.11}Ti_{0.885}Nb_{0.005}O_3$	70	0.41(@333K) 0.30(@333K)	Maxwell LGD	0.14(@RT) 0.145(@348K)	68.18(@RT) 76.35(@358K)	this work
$BaSn_{0.105}Ti_{0.895}O_3$	20	0.61(@301K)	Maxwell			[38]
$Ba_{0.995}Ce_{0.005}Ti_{0.99}Mn_{0.01}O_3$	30	1.22(@393K)	Maxwell	~0.076(@RT)	~40(@RT)	[17]
$Ba_{0.97}Ce_{0.03}Ti_{0.99}Mn_{0.01}O_3$	30	0.41(@328K)	Maxwell	0.11(@RT)	65(@RT)	[17]
$Ba_{0.85}Ca_{0.15}Zr_{0.10}Ti_{0.90}O_3$	6.5	0.109(@363K)	Maxwell	0.014(@393K)	80(@393K)	[39]
$BaTi_{0.99}In_{0.05}O_{2.975}$	36	0.42(@314K)	Maxwell			[40]
$(K_{0.5}Na_{0.5})_{0.096}(Sr_{0.6}Ba_{0.4})_{0.952}Nb_2O_6$	30	0.3(@406K)	Maxwell			[41]
$BaTiO_3$+5wt%glass	88			0.25(@RT)		[42]
$BaTiO_3$+7wt%glass	88			0.32(@RT)		[42]
$0.095BiScO_3 - 0.905Ba_{0.78-\delta}Ca_{0.22-\delta}Sn_{2\delta}Ti_{0.96}Sn_{0.04}O_3$ (δ=0.0025)	100			0.55(@233K)	91(@323K)	[43]
$0.95BaTiO_3$–$0.05Bi(Zn_{2/3}Nb_{1/3})O_3$	70			~0.33(@RT)	~40(@RT)	[44]
$0.9BaTiO_3$–$0.1Bi(Zn_{2/3}Nb_{1/3})O_3$	70			~0.26(@RT)	~93.5(@RT)	[44]

"RT" represents room temperature

polarization in a dominant way rather than the local stress and charge fluctuation.

5 Conclusions

In summary, the ECE of Mn or Nb doped Ba(Sn, Ti)O_3 relaxor ferroelectrics has been evaluated using Maxwell relations and LGD thermodynamic theory. The effect of the heterovalent substitution such as acceptor doping and donor doping on the EC response and energy storage performance of this system has been clarified. The introduction of aliovalent Mn or Nb elements into Ti site would regulate both the EC and energy storage behaviors, and the enhanced EC response, recoverable energy storage density and efficiency can be observed in 0.5 % Mn-doped Ba(Sn, Ti)O_3 ceramics. These results demonstrate that the tunable electrocaloric effect and energy storage performance can be achieved by the acceptor or the donor doping in Ba(Sn, Ti)O_3 relaxor ferroelectrics.

Acknowledgements The authors acknowledge the financial support by National Natural Science Foundation of China (Grant No. 91963116), by Natural Science Foundation of Shanghai (Grant No. 19ZR1411900), by the opening project of Key Laboratory of Inorganic Functional Materials and Devices, Chinese Academy of Sciences (Grant No. KLIFMD201707), and by the opening project of Key Laboratory of Materials Physics, Institute of Solid State Physics, Chinese Academy of Sciences (Grant No. 2018KLMP01).

Data availability The data that support the findings of this study are available from the corresponding author upon reasonable request.

Declarations

Conflicts of interest There are no conflicts of interest to declare.

References

1. N. Setter, D. Damjanovic, L. Eng, G. Fox, S. Gevorgian, S. Hong, A. Kingon, H. Kohlstedt, N.Y. Park, G.B. Stephenson, I. Stolitchnov, A.K. Taganstev, D.V. Taylor, T. Yamada, S. Streiffer, Ferroelectric thin films: Review of materials, properties, and applications. J. Appl. Phys. **100**(5), 051606 (2006). https://doi.org/10.1063/1.2336999
2. H. Kim, Y. Tadesse, S. Priya, *Piezoelectric Energy Harvesting. Energy Harvesting Technologies* (Springer US, New York, 2009). https://doi.org/10.1007/978-0-387-76464-1_1
3. R.J. Ma, Z.Y. Zhang, K.W. Tong, D. Huber, R. Kornbluh, Y.S. Ju, Q.B. Pei, Highly efficient electrocaloric cooling with electrostatic actuation. Science **357**(6356), 1130–1134 (2017). https://doi.org/10.1126/science.aan5980
4. Q.M. Zhang, T. Zhang, The refrigerant is also the pump. Science **357**(6356), 1094–1095 (2017). https://doi.org/10.1126/science.aao2438
5. B. Neese, B. Chu, S.-G. Lu, Y. Wang, E. Furman, Q.M. Zhang, Large electrocaloric effect in ferroelectric polymers near room temperature. Science **321**(5890), 821–823 (2008). https://doi.org/10.1126/science.1159655
6. A.S. Mischenko, Q. Zhang, J.F. Scott, R.W. Whatmore, N.D. Mathur, Giant electrocaloric effect in thin-film $PbZr_{0.95}Ti_{0.05}O_3$. Science **311**(5765), 1270–1271 (2006). https://doi.org/10.1126/science.1123811
7. L. Zhao, X.Q. Ke, Z.J. Zhou, X.Q. Liao, J.J. Li, Y. Wang, M. Wu, T.Y. Li, Y. Bai, X.B. Ren, Large electrocaloric effect over a wide temperature range in $BaTiO_3$-modified lead-free ceramics. J. Mater. Chem. C **7**(5), 1353–1358 (2019). https://doi.org/10.1039/c8tc06110f
8. G.Z. Zhang, X.S. Zhang, H.B. Huang, J.J. Wang, Q. Li, L.Q. Chen, Q. Wang, Toward wearable cooling devices: Highly flexible electrocaloric $Ba_{0.67}Sr_{0.33}TiO_3$ nanowire arrays. Adv. Mater. **28**(24), 4811–4816 (2016). https://doi.org/10.1002/adma.201506118
9. Z.K. Liu, X. Li, Q.M. Zhang, Maximizing the number of coexisting phases near invariant critical points for giant electrocaloric and electromechanical responses in ferroelectrics. Appl. Phys. Lett. **101**(8), 082904 (2012). https://doi.org/10.1063/1.4747275
10. Y. Liu, J.F. Scott, B. Dkhil, Some strategies for improving caloric responses with ferroelectrics. APL Mater **4**(6), 064109 (2016). https://doi.org/10.1063/1.4954056
11. Y. Hou, L. Yang, X. Qian, T. Zhang, Q.M. Zhang, Electrocaloric response near room temperature in Zr- and Sn-doped $BaTiO_3$ systems. Philos. Transact. A Math. Phys. Eng. Sci. **374**(2074), 1–9 (2016). https://doi.org/10.1098/rsta.2016.0055
12. X.M. Chen, X.Z. Ruan, K.Y. Zhao, X.Q. He, J.T. Zeng, Y.S. Li, L.Y. Zheng, C.H. Park, G.R. Li, Low sintering temperature and high piezoelectric properties of Li-doped (Ba,Ca)(Ti,Zr)O_3 lead-free ceramics. J. Alloy. Compd. **632**, 103–109 (2015). https://doi.org/10.1016/j.jallcom.2015.01.088
13. X.Q. Liu, T.T. Chen, M. Sen Fu, Y.J. Wu, X.M. Chen, Electrocaloric effects in spark plasma sintered $Ba_{0.7}Sr_{0.3}TiO_3$-based ceramics: Effects of domain sizes and phase constitution. Ceram. Int. **40**(7), 11269–11276 (2014). https://doi.org/10.1016/j.ceramint.2014.03.175
14. J.N. Li, D.W. Zhang, S.Q. Qin, T.Y. Li, M. Wu, D. Wang, Y. Bai, X.J. Lou, Large room-temperature electrocaloric effect in lead-free $BaHf_xTi_{1-x}O_3$ ceramics under low electric field. Acta Mater. **115**, 58–67 (2016). https://doi.org/10.1016/j.actamat.2016.05.044
15. K.S. Srikanth, R. Vaish, Enhanced electrocaloric, pyroelectric and energy storage performance of $BaCe_xTi_{1-x}O_3$ ceramics. J. Eur. Ceram. Soc. **37**(13), 3927–3933 (2017). https://doi.org/10.1016/j.jeurceramsoc.2017.04.058
16. Z.P. Xu, H. Qiang, Enhanced electrocaloric effect in Mn plus Y co-doped BST ceramics near room temperature. Mater. Lett. **191**, 57–60 (2017). https://doi.org/10.1016/j.matlet.2016.12.120
17. S.J. Liu, Q.D. Xie, L.X. Zhang, Y.Y. Zhao, X. Wang, P. Mao, J.P. Wang, X.J. Lou, Tunable electrocaloric and energy storage behavior in the Ce, Mn hybrid doped $BaTiO_3$ ceramics. J. Eur. Ceram. Soc. **38**(14), 4664–4669 (2018). https://doi.org/10.1016/j.jeurceramsoc.2018.06.020
18. W.P. Cao, W.L. Li, Y. Feng, T. Bai, Y.L. Qiao, Y.F. Hou, T.D. Zhang, Y. Yu, W.D. Fei, Defect dipole induced large recoverable strain and high energy-storage density in lead-free $Na_{0.5}Bi_{0.5}TiO_3$-based systems. Appl. Phys. Lett. **108**(20), 202902 (2016). https://doi.org/10.1063/1.4950974
19. B.J. Chu, X. Zhou, K.L. Ren, B. Neese, M.R. Lin, Q. Wang, F. Bauer, Q.M. Zhang, A dielectric polymer with high electric energy density and fast discharge speed. Science **313**(5785), 334–336 (2006). https://doi.org/10.1126/science.1127798
20. N. Horchidan, A.C. Ianculescu, C.A. Vasilescu, M. Deluca, V. Musteata, H. Ursic, R. Frunza, B. Malic, L. Mitoseriu, Multiscale study of ferroelectric-relaxor crossover in $BaSn_xTi_{1-x}O_3$ ceramics.

J. Eur. Ceram. Soc. **34**(15), 3661–3674 (2014). https://doi.org/10.1016/j.jeurceramsoc.2014.06.005
21. M. Naderer, T. Kainz, D. Schuetz, K. Reichmann, The influence of Ti-nonstoichiometry in $Bi_{0.5}Na_{0.5}TiO_3$. J. Eur. Ceram. Soc. **34**(3), 663–667 (2014). https://doi.org/10.1016/j.jeurceramsoc.2013.10.010
22. U. Prah, M. Wencka, T. Rojac, A. Bencan, H. Ursic, $Pb(Fe_{0.5}Nb_{0.5})O_3$-$BiFeO_3$-based multicalorics with room-temperature ferroic anomalies. J. Mater. Chem. C **8**(32), 11282–11291 (2020). https://doi.org/10.1039/d0tc02329a
23. Y.H. Dong, H.B. Yang, L. Zhang, X.Y. Li, D. Ding, X.H. Wang, J. Li, J.G. Li, I.W. Chen, Ultra-uniform nanocrystalline materials via two-step sintering. Adv. Funct. Mater. **31**(1), 2007750 (2021). https://doi.org/10.1002/adfm.202007750
24. Y. Bai, X. Han, L.J. Qiao, Effect of donor doping in B sites on the electrocaloric effect of $BaTi_{1-x}Nb_xO_3$ ceramics. RSC Adv. **5**(88), 71873–71877 (2015). https://doi.org/10.1039/c5ra11784d
25. S. Merselmiz, Z. Hanani, D. Mezzane, M. Spreitzer, A. Bradesko, D. Fabijan, D. Vengust, M.B. Amjoud, L. Hajji, Z. Abkhar, A.G. Razumnaya, B. Rozic, I.A. Luk'yanchuk, Z. Kutnjak, High energy storage efficiency and large electrocaloric effect in lead-free $BaTi_{0.89}Sn_{0.11}O_3$ ceramic. Ceram. Int. **46**(15), 23867–23876 (2020). https://doi.org/10.1016/j.ceramint.2020.06.163
26. P. Ren, Z. Liu, Q. Wang, B. Peng, S. Ke, H. Fan, G. Zhao, Large nonlinear dielectric behavior in $BaTi_{(1-x)}Sn_xO_{(3)}$. Sci. Rep. **7**, 6693 (2017). https://doi.org/10.1038/s41598-017-07192-x
27. C. Mao, S. Yan, S. Cao, C. Yao, F. Cao, G. Wang, X. Dong, X. Hu, C. Yang, Effect of grain size on phase transition, dielectric and pyroelectric properties of BST ceramics. J. Eur. Ceram. Soc. **34**(12), 2933–2939 (2014). https://doi.org/10.1016/j.jeurceramsoc.2014.04.005
28. Z.T. Yang, F. Gao, H.L. Du, L. Jin, L.L. Yan, Q.Y. Hu, Y. Yu, S.B. Qu, X.Y. Wei, Z. Xu, Y.J. Wang, Grain size engineered lead-free ceramics with both large energy storage density and ultrahigh mechanical properties. Nano Energy **58**, 768–777 (2019). https://doi.org/10.1016/j.nanoen.2019.02.003
29. P.Y. Zhao, H.X. Wang, L.W. Wu, L.L. Chen, Z.M. Cai, L.T. Li, X.H. Wang, High-performance Relaxor ferroelectric materials for energy storage applications. Adv. Energy Mater. **9**(17), 1803048 (2019). https://doi.org/10.1002/aenm.201803048
30. S.J. Liu, L.X. Zhang, J.P. Wang, Y.Y. Zhao, X. Wang, Abnormal Curie temperature behavior and enhanced strain property by controlling substitution site of Ce ions in $BaTiO_3$ ceramics. Ceram. Int. **43**(14), 10683–10690 (2017). https://doi.org/10.1016/j.ceramint.2017.04.164
31. X.Y. Ye, Y.M. Li, J.J. Bian, Dielectric and energy storage properties of Mn-doped $Ba_{0.3}Sr_{0.475}La_{0.12}Ce_{0.03}TiO_3$ dielectric ceramics. J. Eur. Ceram. Soc. **37**(1), 107–114 (2017). https://doi.org/10.1016/j.jeurceramsoc.2016.08.002
32. Y. Hou, J.C. Li, J.F. Ding, T.T. Ye, R.H. Liang, Giant electrocaloric response in compositional manipulated $BaTiO_3$ relaxor-ferroelectric system. J. Appl. Phys. **127**(6), 064103 (2020). https://doi.org/10.1063/1.5142635
33. Y. Liu, J.F. Scott, B. Dkhil, Direct and indirect measurements on electrocaloric effect: Recent developments and perspectives. Appl. Phys. Rev. **3**(3), 031102 (2016). https://doi.org/10.1063/1.4958327
34. M. Sanlialp, Z. Luo, V.V. Shvartsman, X. Wei, Y. Liu, B. Dkhil, D.C. Lupascu, Direct measurement of electrocaloric effect in lead-free $Ba(Sn_xTi_{1-x})O_3$ ceramics. Appl. Phys. Lett. **111**(17), 173903 (2017). https://doi.org/10.1063/1.5001196
35. G. Akcay, S.P. Alpay, G.A. Rossetti Jr., J.F. Scott, Influence of mechanical boundary conditions on the electrocaloric properties of ferroelectric thin films. J. Appl. Phys. **103**(2), 024104 (2008). https://doi.org/10.1063/1.2831222
36. R. Pirc, Z. Kutnjak, R. Blinc, Q.M. Zhang, Electrocaloric effect in relaxor ferroelectrics. J. Appl. Phys. **110**(7), 074113 (2011). https://doi.org/10.1063/1.3650906
37. X. Li, S.-G. Lu, X.-Z. Chen, H. Gu, X. Qiana, Q.M. Zhang, Pyroelectric and electrocaloric materials. J. Mater. Chem. C **1**(1), 23–37 (2013). https://doi.org/10.1039/c2tc00283c
38. Z. Luo, D. Zhang, Y. Liu, D. Zhou, Y. Yao, C. Liu, B. Dkhil, X. Ren, X. Lou, Enhanced electrocaloric effect in lead-free $BaTi_{1-x}Sn_xO_3$ ceramics near room temperature. Appl. Phys. Lett. **105**(10), 102904 (2014). https://doi.org/10.1063/1.4895615
39. Z. Hanani, D. Mezzane, M. Amjoud, A.G. Razumnaya, S. Fourcade, Y. Gagou, K. Hoummada, M. El Marssi, M. Goune, Phase transitions, energy storage performances and electrocaloric effect of the lead-free $Ba_{0.85}Ca_{0.15}Zr_{0.10}Ti_{0.90}O_3$ ceramic relaxor. J. Mater. Sci. Mater. Electron. **30**(7), 6430–6438 (2019). https://doi.org/10.1007/s10854-019-00946-5
40. Y. Zhao, X.Q. Liu, S.Y. Wu, X.M. Chen, Effect of phase transition on electrocaloric effect in Indium substituted $BaTiO_3$ ceramics. J. Alloy. Compd. **822**, 153632 (2020). https://doi.org/10.1016/j.jallcom.2019.153632
41. A. Kurnia, N. Emriadi, Mufti, U. Zulhadjri, Adem, Electrocaloric effect of alkali co-substituted $Sr_{0.6}Ba_{0.4}Nb_2O_6$ ceramics. J. Alloy. Compd. **844**, 156132 (2020). https://doi.org/10.1016/j.jallcom.2020.156132
42. X.R. Wang, Y. Zhang, X.Z. Song, Z.B. Yuan, T. Ma, Q. Zhang, C.S. Deng, T.X. Liang, Glass additive in barium titanate ceramics and its influence on electrical breakdown strength in relation with energy storage properties. J. Eur. Ceram. Soc. **32**(3), 559–567 (2012). https://doi.org/10.1016/j.jeurceramsoc.2011.09.024
43. S. Nayak, S. Venkateshwarlu, A.S. Budisuharto, M.R.V. Jorgensen, O. Borkiewicz, K.A. Beyer, A. Pramanick, Effect of A-site substitutions on energy storage properties of $BaTiO_3$-$BiScO_3$ weakly coupled relaxor ferroelectrics. J. Am. Ceram. Soc. **102**(10), 5919–5933 (2019). https://doi.org/10.1111/jace.16449
44. L.W. Wu, X.H. Wang, L.T. Li, Lead-free $BaTiO_3$-$Bi(Zn_{2/3}Nb_{1/3})O_3$ weakly coupled relaxor ferroelectric materials for energy storage. RSC Adv. **6**(17), 14273–14282 (2016). https://doi.org/10.1039/c5ra21261h
45. L.X. Zhang, X.B. Ren, Aging behavior in single-domain Mn-doped $BaTiO_3$ crystals: Implication for a unified microscopic explanation of ferroelectric aging. Phys. Rev. B **73**(9), 094121 (2006). https://doi.org/10.1103/Physrevb.73.094121
46. M. Blömker, E. Erdem, S. Li, S. Weber, A. Klein, J. Rödel, T. Frömling, Defect structure of doped lead-free $0.9(Bi_{0.5}Na_{0.5})TiO_3$ – $0.1(Bi_{0.5}K_{0.5})TiO_3$ piezoceramics. J. Am. Ceram. Soc. **99**(2), 543–550 (2016). https://doi.org/10.1111/jace.13999
47. Y. Li, Y. Tang, J. Chen, X. Zhao, L. Yang, F. Wang, Z. Zeng, H. Luo, Enhanced pyroelectric properties and thermal stability of Mn-doped $0.29Pb(In_{1/2}Nb_{1/2})O_3$-$0.29Pb(Mg_{1/3}Nb_{2/3})O_3$-$0.42PbTiO_{(3)}$ single crystals. Appl. Phys. Lett. **112**(17) (2018). https://doi.org/10.1063/1.5024286
48. Q. Zhang, M. Fan, S. Jiang, T. Yang, X. Yao, Enhanced antiferroelectric and electric-induced pyroelectric properties of Mn-substitued $(Pb_{0.832}Ba_{0.138}La_{0.02})(Zr_{0.7}Ti_{0.05}Sn_{0.25})O_3$ ceramics. Appl. Phys. Lett. **101**(6) (2012). https://doi.org/10.1063/1.4744948
49. Y.X. Tang, Z.Y. Shen, S.J. Zhang, T.R. Shrout, Improved pyroelectric properties of $CaBi_4Ti_4O_{15}$ ferroelectrics ceramics by Nb/Mn Co-Doping for Pyrosensors. J. Am. Ceram. Soc. **99**(4), 1294–1298 (2016). https://doi.org/10.1111/jace.14075